Design and Optimization of High-frequency Transformer for Isolated Single-Stage Three-Phase AC/DC Converter using Bidirectional Switches

Isaac Wong, Ramandeep Narwal, Subhashish Bhattacharya, B. Jayant Baliga, and Douglas C. Hopkins
Department of Electrical and Computer Engineering
North Carolina State University, NC 27606, USA
twong3@ncsu.edu, rnarwal@ncsu.edu, sbhatta4@ncsu.edu, bjbaliga@ncsu.edu, dchopkins@ncsu.edu

***Abstract*—This paper presents the design and optimization of the high-frequency transformer for an isolated single-stage three-phase AC/DC converter enabled by the 4H-SiC BiDirectional Field Effect Transistor (BiDFET). Non-dominated Sorting Genetic Algorithm II (NSGA-II) is used to perform a multiobjective optimization to minimize loss, weight, and volume. A 20 kW, 50 kHz hardware prototype based on the selected optimal point is characterized by a power amplifier. The finite element analysis simulation results are also presented to validate the core magnetic flux density and winding electric field strength. The experimental prototype was tested at 800 V_{dc}/480 V_{rms} at 10 kW rated power.**

***Index Terms*—BiDFET, High-frequency transformer, Multiobjective optimization**

I. Introduction

The first monolithic SiC four-quadrant ($4Q$) switch has been fabricated with two 1.2 kV 4H-SiC JBSFETs connected in a common-drain configuration [1]. An isolated AC/DC converter for grid-tied photovoltaic (PV) three-phase commercial application shown as Fig 1, is proposed to demonstrate the feasibility and to showcase the system-level benefits of using monolithic BiDFET [2]. The proposed converter has a full-bridge inverter using 2-quadrant switches on the PV-side, whereas the matrix converter on the grid-side operates by switching any two-phases during a switching period. Owing to the new switching sequence enabled by the $4Q$ BiDFET, a multi-level staircase voltage is imposed on the isolation transformer, in which the excitation for such converter is different from a traditional DAB converter [3]. The converter can be operated as an inverter or as a rectifier depending on the application. In this work, the inverter mode is used to interface the 800 V_{dc} PV with the 480 V_{rms} power grid.

Safety requirements are one of the most important aspects of a PV system due to the high parasitic capacitance between the solar PV cells and the grounded conductive chassis. Despite the drawbacks of increasing cost and reducing the system efficiency, the use of a high-frequency transformer lowers the leakage current by providing galvanic isolation between the grid and the PV panels [4]. As a common industry practice, the PV systems are expected to a service life of at least 25 years, and yet the systems have to be competitively priced. The safety measures provided by the isolation transformer are often desired, if not required. Thus, it is imperative to minimize the transformer loss, weight, and volume, and hence alleviating the penalty in cost to allow the isolated inverter topologies to be a competitive solution to their transformerless counterparts.

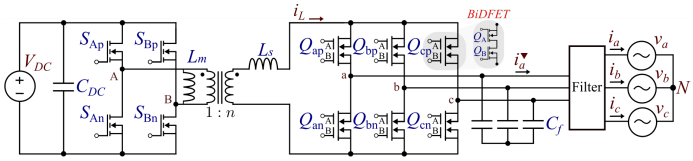

Fig. 1: Isolated BiDFET-enabled three-phase AC/DC converter

TABLE I: Isolated Three-phase AC/DC Converter and High-Frequency Transformer Specifications

Parameters	Value
DC Voltage	800 V_{dc}
Three-phase AC Voltage	480 V_{rms}
Maximum Rated Power	20 kW
Nominal Switching Frequency	50 kHz
Turns-Ratio	0.78
Magnetizing Inductance	>2.5 mH
External Series Inductance	27.6 μH
Maximum Primary Winding Current	34 Arms
Maximum Secondary Winding Current	42 Arms
Maximum Primary Winding Voltage	1200 Vpk
Maximum Secondary Winding Voltage	1200 Vpk
THD	$\leq$ 5%

This article presents the optimization process, the staircase excitation illustration, the hardware prototype of the high-frequency transformer, and the experimental results with the three-phase AC/DC converter. The specifications of the isolated AC/DC converter are listed in Table I.

II. Multiobjective Optimization

A. Optimization Methodology

Advanced optimization algorithms such as the non-sorting genetic algorithm (NSGA-II) have been widely adopted by academia and industry as a tool for optimization problems with more than one objective and with multiple variables and constraints. The controlled, elitist algorithm generates the Pareto front by performing crossover and mutation on the optimization variables, and procreates the next generation based on the Pareto front dominance of the current population. Maintaining a diverse population is critical for the convergence

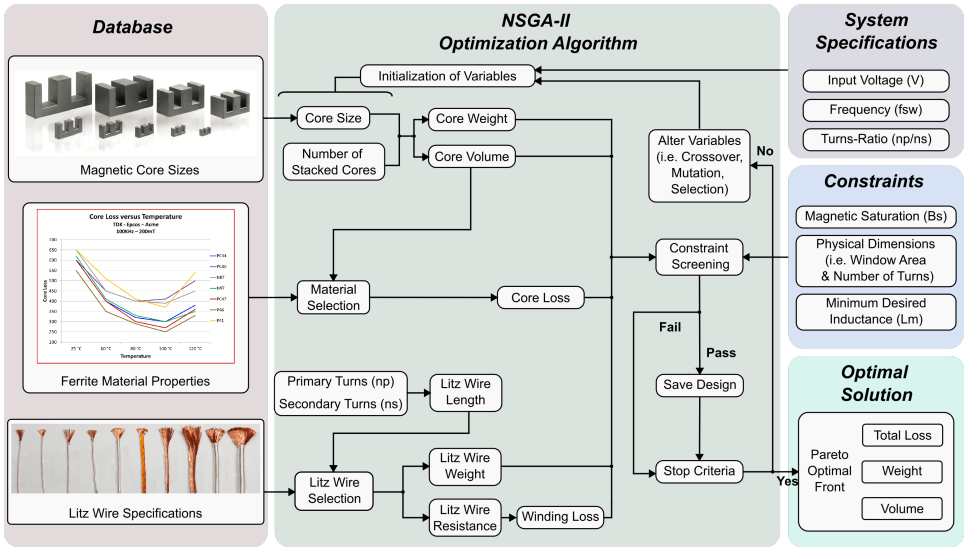

Fig. 2: NSGA-II optimization flow chart

of the Pareto optimal front. The algorithm employs a crowding distance function to estimate the density of elite members of the population on a given front, such that, the diversity of the population is preserved. The optimization process continues until the max number of generations are reached, or the average relative change in best fitness value is less than or equal to the function tolerance [7]. Hence, NSGA-II has been used in this work to minimize the loss, weight, and volume of the high-frequency transformer with multiple physical and magnetic constraints. Fig 2 summarizes the optimization process, objectives, constraints, and input specifications. The three objective functions to be minimized can be expressed as

$$\min f_1(x) = \min_{i=1}^{x} \left[\frac{1}{\eta(x)}\right] \tag{1}$$

$$\min f_2(x) = \min_{i=1}^{x} [W(x)] \tag{2}$$

$$\min f_3(x) = \min_{i=1}^{x} [V(x)] \tag{3}$$

B. Core Loss Estimation

Soft magnetic materials are ubiquitous in power magnetics designs for achieving high self-inductance with fewer turns compared to using an air core by providing a low reluctance path for magnetic flux to travel in. At a nominal switching frequency of 50 kHz, ferrite and nanocrystalline material are both prime candidates at such frequency. Considering the path to demonstrate BiDFET at higher frequencies in the future, this design only considers ferrite for its high resistivity and low eddy current loss.

Switching mode power supplies are often excited with a non-sinusoidal waveform, and therefore renders the Steinmetz equation (SE) inaccurate to model magnetic losses. The waveform coefficient Steinmetz equation (WcSE) was proposed to correlate Steinmetz coefficients obtained by sinusoidal excitation to estimate the magnetic losses excited under non-sinusoidal waveforms with the same magnetic flux density and frequency [5]. It has been shown that with a duty cycle D at 0.5, losses modeled by WcSE closely match the experimental data [6]. The time-averaged core loss per unit volume P_V and the total core loss P_{core} are given as follows:

$$P_V = \frac{\pi}{4}(2-D)kf^{\alpha}{B_m}^{\beta} \tag{4}$$

$$P_{core} = P_V V_c n_c \tag{5}$$

where α and β are the Steinmetz coefficients of the magnetic material.

C. Winding Loss Estimation

In order to reduce high-frequency losses caused by the skin and proximity effect, the Litz wire is used for both windings. The winding loss is calculated based on DC and AC copper loss. The DC loss is determined by the dimensions of the winding, the conductor resistance, the number of turns, and the winding current where the AC loss of the Litz wire is a function of the number of individual bundles, the wire diameter of the Litz wire, the individual wire, and the operating frequency.

$$P_{winding} = P_{dc} + P_{ac} \tag{6}$$

$$P_{dc} = nR_{dc}I_{dc}^2 \tag{7}$$

$$P_{ac} = nI_{ac}^2\left[R_{dc}(H + K(\frac{ND_I}{D_o})^2(\frac{D_I\sqrt{f}}{10.44})^4)\right] \tag{8}$$

where f is the operating frequency in Hz, N is the number of strands in the cable, D_I is the diameter of individual strands in inches, D_o is the outer diameter of the Litz wire in inches, K and H are constants given by the manufacturer datasheet.

D. Weight and Volume

The mean length per turn of the transformer windings are determined by the core dimensions and the number of stacked cores n_c. The transformer weight W_{total} and volume V_{total} can then be calculated by

$$W_{total} = (n_c m_c) + (n l_w m_{winding}) \tag{9}$$

$$V_{total} = n_c(w_c\, d_c\, h_c) \tag{10}$$

where m_c denotes the weight per core in gram, n denotes the number of turns, l_w denotes the mean length per turn in meters, $m_{winding}$ denotes the winding weight per unit in gram per meters, and w_c, d_c, h_c are the core width, core depth, and core height, respectively.

E. Window Area

A feasible design must have a sufficient core window area to enclose all winding turns. The total copper area can be approximated by the product of the number of turns n and the wire copper area which must less than the window area.

$$A_{window} > n_p d_{w,p}^2 + n_s d_{w,s}^2 \tag{11}$$

F. Magnetizing Inductance

The soft-switching region of the three-phase AC/DC converter can be extended by having a low impedance magnetizing branch in the high-frequency transformer. Nonetheless, it is desirable to restrict the magnetizing inductance to a desired minimum value to prevent excess losses incurred by high circulating current. By using a magnetic circuit model, the magnetizing inductance L_m is given as

$$L_m = \frac{\mu_0 n_p^2 A_c}{l_e}\left[1 + \frac{l_g}{\sqrt{A_c}} \ln\left(\frac{h_w}{l_g}\right)\right] \tag{12}$$

where l_e is the magnetic path length, l_g is the air gap length, and h_w is the window height.

G. Magnetic Flux Density

The 4-quadrant BiDFETs allow the AC/DC converter to adopt a novel switching scheme. Thereby, the transformer excitation waveform of the BiDFET-enabled converter comprises a multi-level staircase waveform instead of the conventional 2-level waveform of a DAB converter. The root-mean square value of an arbitrary n-level staircase voltage excitation waveform is given by

$$V_{rms} = \sqrt{\frac{1}{T}\sum_{i=1}^{n}\int_{t_i}^{t_{i+1}} V_n^2\, dt} \tag{13}$$

where

The excitation waveform coefficient k can then determined by the ratio of the rms voltage and the average voltage during τ and the switching frequency f

$$k = \frac{V_{rms}}{V_{ave_\tau} \tau f} \tag{14}$$

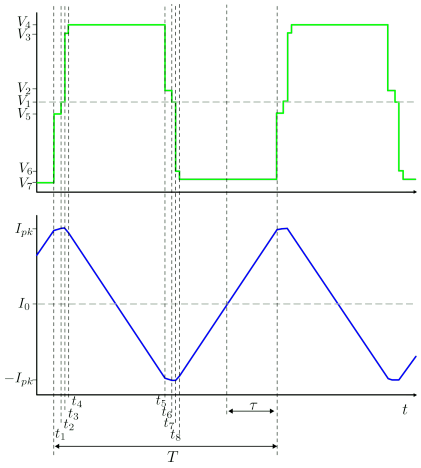

Fig. 3: Transformer voltage and current excitation waveforms

The waveform coefficient of the SiC BiDFET-enable converter ranges from 4.02 to 4.18 extracted from simulation results. Consequently, the maximum core magnetic flux density can be determined by Faraday's law

$$B_m = \frac{V_p}{k\, n_p A_c f} \tag{15}$$

III. Optimization Results

The optimization process described in Fig 2 has been tested using the Viennet function. The Pareto zone shown in Fig 4 exhibits the same distribution and discontinuity between the Pareto optimal variables as reported in [8]. The results of using the test function verifies the fidelity of the proposed optimization process.

The Pareto optimal front of the optimization results is shown in Fig 5, and the selected transformer parameters for all optimal design points are shown in Fig 6. The selected design achieves the second lowest volume and weight, and a core flux density of 0.137 T, which offers a sufficient safety headroom to avoid saturation while testing the novel BiDFET-enabled converter. Table II summarizes the external inductor and the selected Pareto optimal transformer parameters.

IV. Transformer Prototyping and Characterization

The selected optimal transformer design has been built and is shown in Fig 7. A square wave of 50% duty cycle at 50 kHz generated by AE Techron 7224 900-VA power amplifier is used for transformer characterization. The short-circuit excitation voltage and current waveforms are captured 9. The open circuit characterizes the magnetizing inductance to be 4.87 mH by exciting the primary winding while leaving the secondary open. The primary and secondary side leakage inductances have been determined as 10.2 μH and 5.9 μH, respectively. The equivalent leakage inductance referred to the grid side is 12.1 μH. The optimal design is simulated using finite-element analysis to verify the magnetic flux density. The transformer primary winding is excited with the rated

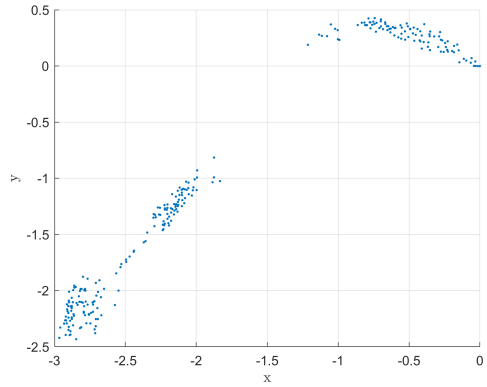

Fig. 4: Viennet test function Pareto optimal variable distribution

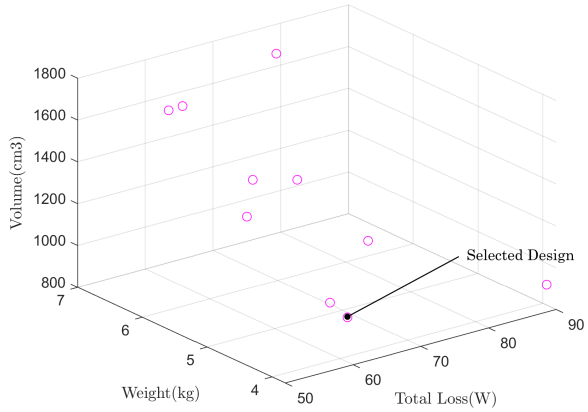

Fig. 5: Pareto optimal front shows the optimal design points with total loss, weight, and volume

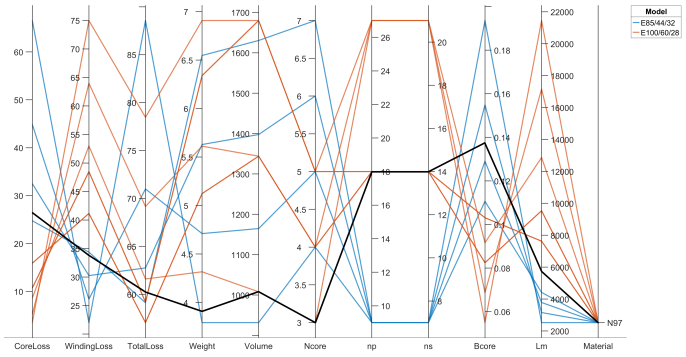

Fig. 6: Transformer parameters of Pareto optimal design points. Each line represents a Pareto optimal design point, and each color represents a corresponding core size indicated in the legend. The selected design is highlighted in black.

TABLE II: Selected Optimal Transformer and Inductor Design for Three-Phase AC/DC Converter

High-Frequency Transformer	Core Material	N97
	Core Size	E100/60/28 x6
	Primary Turns	18
	Secondary Turns	14
	Core Flux Density	0.137 T
	Magnetizing Inductance	5.72 mH
	Core Loss	26.43 W
	Winding Loss	33.82 W
	Total Loss	60.25 W
	Weight	3.91 kg
	Volume	1008 cm^3
Series Inductor	Core Material	3C92
	Core Size	E70/33/32 x4
	Self-Inductance	27.9 uH
	Number of Turns	7
	Core Gap	3.75 mm
	Core Flux Density	0.13 T

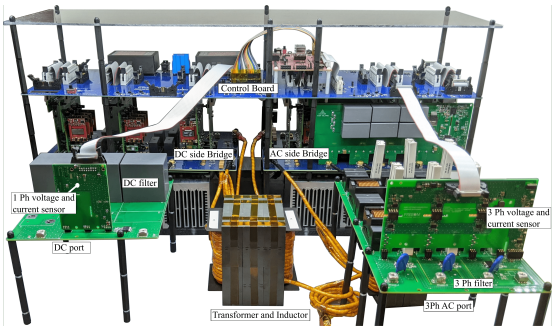

Fig. 7: Transformer hardware prototype with SiC BiDFET-enabled three-phase AC/DC converter

condition to simulate the flux density. Fig 10 shows the bulk of the core limbs at around 0.16 T while the corners of the window area experience flux crowding. The primary and secondary windings have a similar geometry but differ in the number of turns. Thus, the electric field intensities are similar in value. The maximum intensity of the primary winding is 0.47 kV/mm, whereas the secondary winding has a maximum of 0.48 kV/mm as shown in Fig 11. No partial breakdown or partial discharge is expected as the electric field strength is below the breakdown voltage of the polyimide insulation tape and air.

V. Experimental Results

The proposed high-frequency transformer and the isolated single-stage three-phase AC/DC converter have been built and tested at an input of 800 V_{dc}, and an output of 480 V_{rms} at 10 kW. For this paper, the three-phase converter utilized back-to-back connected MOSFETs (C3M0016120K). Fig 12 and 13 demonstrate the staircase waveforms imposed by DC-side full-bridge and AC-side matrix converter across the transformer terminals. The transformer steady-state voltage waveforms comprise a high-frequency multi-level staircase component at the switching frequency and is bounded by a low-frequency envelop. The phase current has a THD of 3.5% which meets

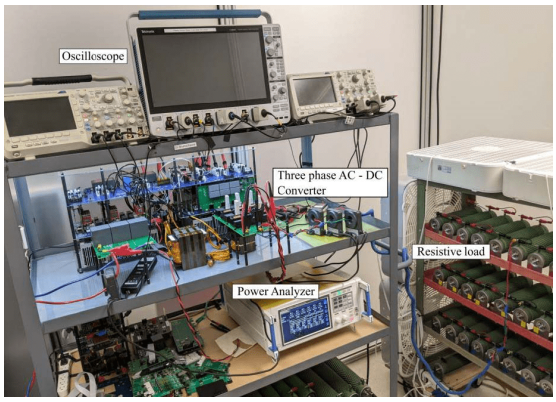

Fig. 8: Test Setup for SiC BiDFET-enabled three-phase AC/DC converter

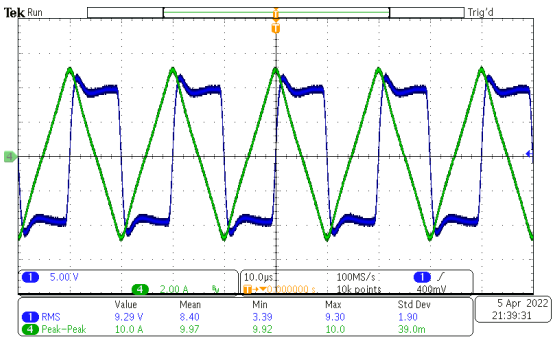

Fig. 9: Short circuit test excitation voltage (blue) and current (green)

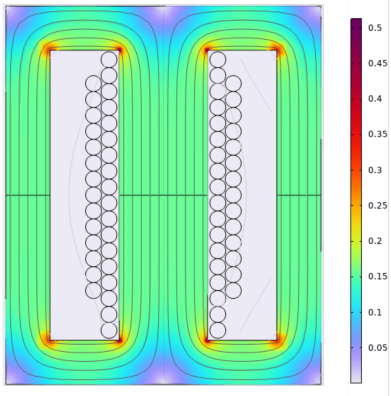

Fig. 10: Simulated transformer flux density shows 0.155 T in the transformer limbs, which is lower than the N97 saturation flux density of 0.41 T at 100°C

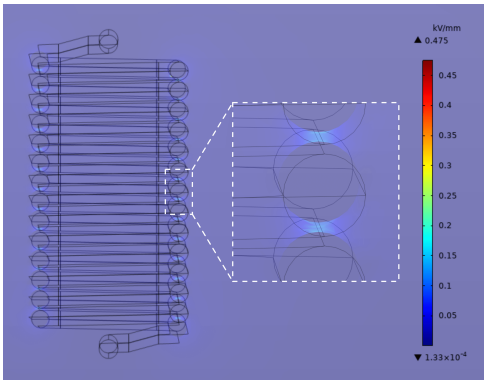

Fig. 11: Simulated electric field strength of primary winding with a worst case voltage of 1200 V shows the maximum E-field of 0.47 kV/mm

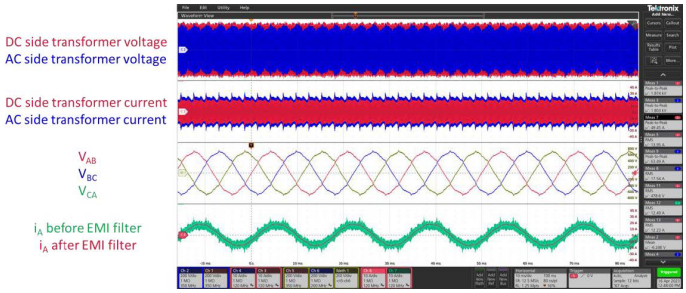

Fig. 12: Transformer voltage and current experimental waveforms at 480 V, 10 kW ouput at 800 Vdc input

the less than 5% limit. The converter steady-state operation has been shown with a peak efficiency of 98.1% at 10 kW.

VI. Conclusion

This paper outlines the optimization of a high-frequency transformer tailored for an isolated single-stage three-phase AC/DC converter, enabled by novel 1.2 kV SiC BiDFET bidirectional switches. Both the design considerations and optimization methodologies are detailed. The Pareto optimal front presents the most favorable designs, and the final choice is determined by evaluating the key parameters across all optimal design points. To confirm that the transformer's magnetic properties meet the desired specifications, its magnetizing and leakage inductance were assessed using a power amplifier. Additionally, a finite-element analysis of the transformer was performed to emulate the magnetic flux density in the core and

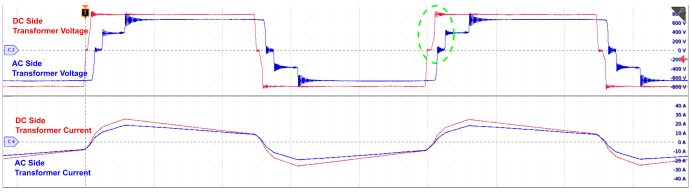

Fig. 13: Transformer voltage and current experimental zoom-in waveforms illustrating the staircase voltage

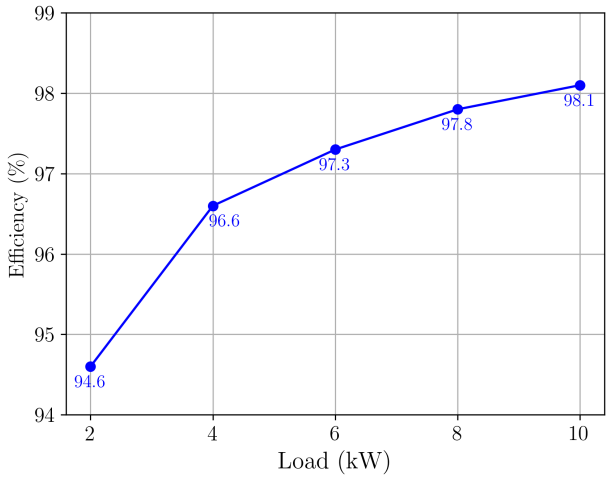

Fig. 14: BiDFET-enabled AC/DC converter efficiency curve from 2 kW to 10 kW

determine the electric field intensity. A prototype of the transformer and the isolated single-stage AC/DC converter enabled by back-to-back commercial MOSFETs was developed. This prototype was tested at an 800 V DC input and 480 V_{rms} three-phase AC output under varying load, achieving a steady-state efficiency of 94.6% at 2 kW to 98.1% at 10 kW.

ACKNOWLEDGMENT

The authors would like to thank the Department of Energy Solar Energy Technologies Office (SETO) for supporting this work.

REFERENCES

[1] K. Han et al., "Monolithic 4-Terminal 1.2 kV/20 A 4H-SiC Bi-Directional Field Effect Transistor (BiDFET) with Integrated JBS Diodes," 2020 32nd International Symposium on Power Semiconductor Devices and ICs (ISPSD), Vienna, Austria, 2020, pp. 242-245, doi: 10.1109/ISPSD46842.2020.9170064.

[2] S. S. Shah et al., "Optimized AC/DC Dual Active Bridge Converter using Monolithic SiC Bidirectional FET (BiDFET) for Solar PV Applications," 2021 IEEE Energy Conversion Congress and Exposition (ECCE), Vancouver, BC, Canada, 2021, pp. 568-575, doi: 10.1109/ECCE47101.2021.9595533.

[3] R. Narwal et al., "Isolated Single-stage Three-phase AC/DC Converter using Bidirectional Switches," in 2023 IEEE Energy Conversion Congress and Exposition (ECCE), 2023.

[4] R. Hasan, S. Mekhilef, M. Seyedmahmoudian, and B. Horan, "Grid-connected isolated PV microinverters: A review," Renew. Sustain. Energy Rev., vol. 67, pp. 1065–1080, Jan. 2017, doi: 10.1016/j.rser.2016.09.082.

[5] W. Shen, F. Wang, D. Boroyevich, and C. W. Tipton, "Loss Characterization and Calculation of Nanocrystalline Cores for High-Frequency Magnetics Applications," IEEE Trans. Power Electron., vol. 23, no. 1, pp. 475–484, 2008, doi: 10.1109/TPEL.2007.911881.

[6] S. Yue, Y. Li, Q. Yang, X. Yu and C. Zhang, "Comparative Analysis of Core Loss Calculation Methods for Magnetic Materials Under Nonsinusoidal Excitations," in IEEE Transactions on Magnetics, vol. 54, no. 11, pp. 1-5, Nov. 2018, Art no. 6300605, doi: 10.1109/TMAG.2018.2842064.

[7] K. Deb, A. Pratap, S. Agarwal, and T. Meyarivan, "A fast and elitist multiobjective genetic algorithm: NSGA-II," IEEE Trans. Evol. Comput., vol. 6, no. 2, pp. 182–197, Apr. 2002, doi: 10.1109/4235.996017.

[8] R. VIENNET, C. FONTEIX, and I. MARC, "Multicriteria optimization using a genetic algorithm for determining a Pareto set," Int. J. Syst. Sci., vol. 27, no. 2, pp. 255–260, Feb. 1996, doi: 10.1080/00207729608929211.